ChemPubSoc Europe

DOI: 10.1002/chem.201904379

CHEMISTRY A European Journal Full Paper

Copper Complexes

Copper(I) Phosphinooxazoline Complexes: Impact of the Ligand Substitution and Steric Demand on the Electrochemical and Photophysical Properties

Robin Giereth,[a] Alexander K. Mengele,[a] Wolfgang Frey,[b] Marvin Kloß,[c] Andreas Steffen,[c] Michael Karnahl,*[b] and Stefanie Tschierlei*[a]

Abstract: A series of seven homoleptic Cu^{I} complexes based on hetero-bidentate P^N ligands was synthesized and comprehensively characterized. In order to study structure–property relationships, the type, size, number and configuration of substituents at the phosphinooxazoline (phox) ligands were systematically varied. To this end, a combination of X-ray diffraction, NMR spectroscopy, steady-state absorption and emission spectroscopy, time-resolved emission spectroscopy, quenching experiments and cyclic voltammetry was used to assess the photophysical and electrochemical properties. Furthermore, time-dependent density functional theory calculations were applied to also analyze the excited state structures and characteristics. Surprisingly, a strong dependency on the chirality of the respective P^N ligand was found, whereas the specific kind and size of the different substituents has only a minor impact on the properties in solution. Most importantly, all complexes except **C3** are photostable in solution and show fully reversible redox processes. Sacrificial reductants were applied to demonstrate a successful electron transfer upon light irradiation. These properties render this class of photosensitizers as potential candidates for solar energy conversion issues.

Introduction

Photoactive Cu^{I} complexes are considered as a highly promising alternative to traditional systems based on noble metals such as ruthenium, iridium, rhenium or platinum.[1–5] Indeed, Cu^{I} compounds were already successfully applied as photosensitizers in the light-driven reduction of protons to H_2,[6–11] as photoredoxcatalysts for organic transformations[12–16] or in devices such as organic light-emitting diodes (OLEDs),[17–22] dye-sensitized solar cells (DSSCs)[23–26] and light-emitting electrochemical cells (LECs).[27,28] Unfortunately, a limited stability under operating conditions still hampers their large-scale application in molecular solar energy conversion schemes.[21,29–34] It is known, that in particular heteroleptic Cu^{I} complexes of the type $[(P\text{^}P)Cu(N\text{^}N)]^{+}$ (with P^P representing a diphosphine and N^N a diimine ligand) can undergo ligand exchange reactions in solution upon light irradiation.[29,31,33–35] This is mainly caused by the formation of thermodynamically more favored homoleptic bisdiimine complex $[Cu(N\text{^}N)_2]^{+}$.[29,31,33–35] Hence, this drawback drove the search and development of novel Cu^{I} complexes with an increased stability, but also having other desired properties like a broad absorption in the visible and a reversible redoxchemistry.[4,36–40]

One possible option to achieve this aim is the replacement of the original P^P ligand by a heterobidentate P^*N*-ligand.[17,41] Particularly, the combination of a *N*-heteroaryl moiety, which possesses a wide range of tunable electronic properties and a soft phosphine donor seems promising.[41,42] Several Cu^{I} complexes based on different types of P^N ligands, mainly as multinuclear cuprous halide complexes, have already been prepared and investigated.[43–53] In these examples the phosphine unit is either directly bound to the *N*-heteroaryl moiety (e.g., 2-(diphenylphosphino)-pyridine[46,49] or 8-(diphenylphosphino)-quinoline[44,45]) or connected via an aliphatic spacer (e.g. 2-[2-(diphenylphosphino)-ethyl]-pyridine[51,53]). Consequently, the previous examples are typically bridging or only monodentate ligands due to the small bite angle.[44–46,49,51,53,54]

[a] *R. Giereth, A. K. Mengele, Dr. S. Tschierlei*
Institute of Inorganic Chemistry I, Ulm University
Albert-Einstein-Allee 11, 89081 Ulm (Germany)
E-mail: stefanie.tschierlei@uni-ulm.de
Homepage: www.tschierlei-group.de

[b] *Dr. W. Frey, Dr. M. Karnahl*
Institute of Organic Chemistry, University of Stuttgart
Pfaffenwaldring 55, 70569 Stuttgart (Germany)
E-mail: michael.karnahl@oc.uni-stuttgart.de
Homepage: www.karnahl-group.de

[c] *M. Kloß, Prof. Dr. A. Steffen*
Faculty of Chemistry and Chemical Biology
TU Dortmund University, Otto-Hahn-Strasse 6
44227 Dortmund (Germany)

Supporting information and the ORCID identification number(s) for the author(s) of this article can be found under: https://doi.org/10.1002/chem.201904379: General information on the experimental and synthetic details, crystallographic data, NMR and UV/vis spectra, cyclic voltammograms as well as results of the (TD-)DFT calculations.

Moreover, these systems still suffer from a limited stability.[21,55,56]

In contrast, Zeng et al. found that 1,2-phenyl-bridged P^*N*-ligands can form phosphorescent and stable Cu^{I} complexes in solution and in the solid state.[57] Nevertheless, the impact of different substituents, steric effects and chirality on the electrochemistry and photophysics of copper P^N complexes has not been studied in detail yet.

In a previous study we showed for the first time, that a phosphinooxazoline (phox) based P^N ligand enables stable mononuclear Cu^{I} complexes with interesting photophysical properties.[41] Moreover, also the ability of these complexes to act as photosensitizers for the light-driven production of H_2 was demonstrated.[41] Hence, the impact of the spatial arrangement and steric demand in such phox ligands on the properties of the resulting Cu^{I} complexes is of high interest. In consequence, a systematic series of seven homoleptic Cu^{I} complexes (Figure 1) with different size, type and number of substituents at the oxazoline moiety was prepared.

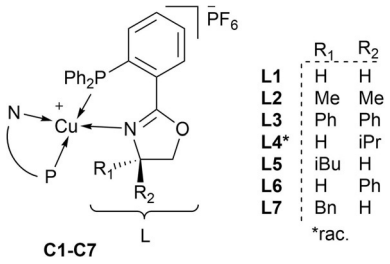

Figure 1. General structure of the ligands **L1** to **L7** and the resulting homoleptic Cu^{I} complexes **C1** to **C7**.

Following, a combination of NMR spectroscopy, X-ray analysis, cyclic voltammetry, absorption and emission spectroscopy as well as density functional theory (DFT) calculations was used to identify structure–property relationships. The presence of single crystals of all compounds enabled a detailed discussion of their solid state structures. In addition, time-resolved emission spectroscopy and time-dependent DFT (TD-DFT) calculations were applied to also examine excited state properties. Most remarkably a dependence of the complex properties on the chirality of the respective P^N ligand was found. Finally, measurements with sacrificial reductants on representative complexes were performed to demonstrate successful electron transfer upon light irradiation. All in all, the gained knowledge paves the way to improved photoactive Cu^{I} complexes, which might be used in solar energy conversion schemes in the future.

Results and Discussion

Synthesis and Structural Characterization

A broad variety of phox ligands were prepared (see Figure 1) to allow for a comprehensive evaluation of the ligand impact on the ground and excited state properties of the resulting Cu^{I} complexes. Main attention was given to the steric influence of the different substituents at the 4-position of the 2-oxazoline (4,5-dihydrooxazole) moiety. This position was chosen for modification due to its proximity to the copper center, because this likely has a strong impact on the geometry as well as on excited state relaxation processes. A special distinction has been made between derivatives without any substituents (**L1**), with only one substituent (**L4**–**L7**) and two substituents (**L2**–**L3**) at the 2-oxazoline (Figure 1). Furthermore, phox ligands with aliphatic (Me, *i*Pr, *i*Bu) and aromatic substituents (Ph, Bn) were prepared. While **L1**, **L2** and **L4**–**7** are literature known, **L3** was specifically designed for this study. It is also worth noting, that the ligands **L4**–**L7** possess a chirality center at the 4-position of the 2-oxazoline. The synthesis of the ligands **L1**, **L2**, **L5** and **L6** was performed following a synthesis procedure from literature,[41,58,59] starting from the corresponding and commercially available chiral amino alcohols (see Scheme 1). These

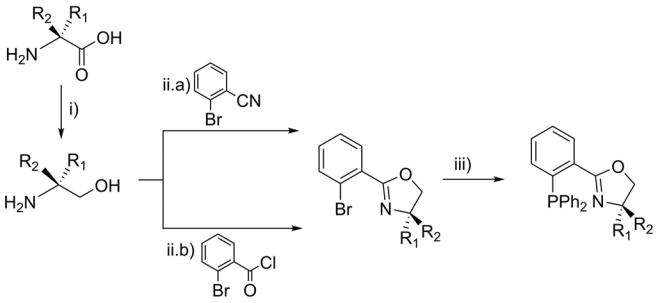

Scheme 1. Overview of the common synthesis procedure of the ligands **L1** to **L7** either starting from the respective amino acids or the amino alcohols. i) Reduction: $LiAlH_4$, THF,[60] ii.a) Witte–Seeliger reaction: $ZnCl_2$, PhCl,[58] ii.b) step 1: $NaHCO_3$, H_2O/DCM; step 2: TsCl, TEA, DCM,[59] iii) Ullman-type coupling: CuI, DMEDA, Cs_2CO_3, toluene.[59]

amino alcohols were first reacted in a Witte–Seeliger reaction[58] to the aryl-bromide precursor and then converted to the corresponding phox ligands via an Ullman-type coupling (Scheme 1).[59] In contrast, the preparation of **L4** and **L7** was done using the easily accessible amino acids (i.e., D,L-valine, (*S*)-phenylalanine) as natural feedstock, while for **L3** a commercially available amino acid (2,2-diphenylglycine) was utilized. For these three ligands the required aryl-bromide precursors were obtained from the respective amino acids in a two-step reaction using $LiAlH_4$ for reduction[60] followed by the acid catalyzed reaction with bromo-benzoylchloride (Scheme 1).[59] In the case of **L4** a racemic mixture of the *R* and *S* configured isomer was obtained, while the ligands **L5**–**L7** are chiral and the stereochemical information of the educts was preserved This means that **L6** is *R* configured and **L5** as well as **L7** possess a *S* configuration at the stereocenter.

The ligands **L1**–**L7** were subsequently coordinated to a Cu^{I} center by a ligand substitution reaction using the $[Cu(MeCN)_4]PF_6$ adduct (MeCN = acetonitrile) as a precursor. Following a general synthesis procedure $[Cu(MeCN)_4]PF_6$ (1 equiv) and the respective phox ligand (**L1**–**L7**, 2 equiv) were suspended in dry dichloromethane and heated to reflux for 5 h under argon atmosphere. After isolation and purification, the homoleptic Cu^{I} complexes **C1**–**C7** of the type $[Cu(phox)_2]PF_6$ were

obtained as yellow to orange crystals. The obtained yields differ in the range from 11% for **C3** to 60% for **C2** (for further details see the Supporting Information). The much lower yield of **C3** significantly differs from all other complexes and might be caused by steric constraints (two adjacent phenyl groups) and hence kinetic instability in solution. Such instability, for example, substitution reactions in solution, is well known from sterically congested homo- and heteroleptic Cu^{I} complexes.[29,31,33–35]

In a next step the molecular composition and structures of all complexes were confirmed by standard analytical techniques. In the $^{31}P\{^{1}H\}$ NMR spectra all complexes display one single signal in the range between −8.5 (**C2**) and −5.3 ppm (**C6**) (Figure S2), indicating a weak influence of the different substituents. A relatively small and broadened $^{31}P\{^{1}H\}$ NMR signal of **C3** is another indication for a limited stability of this particular complex in solution.

Single crystals suitable for X-ray crystallography of all complexes **C1**–**C7** were either obtained by common diffusion techniques or directly from recrystallization in methanol. The crystallographic data and depiction of all solid-state structures can be found in the Supporting Information (Chapter 4), while only a selection is presented here. For instance, complex **C4** crystallizes in the centrosymmetric space group $P2_1/n$. Consequently, **C4** is therefore invariant under the parity operation P (inversion through a point), which prevents the specification of an absolute structure (i.e., whether it is the *R* or the *S* enantiomer). This is in line with the preparation conditions, where a racemic mixture of **L4** was used for complexation. In contrast, the crystal structures of **C5**–**C7** (Figures 4 and S4), which contain the chiral ligands **L5**–**L7**, have a valid absolute-structure determination (see Flack parameters, Table 1). Structural analysis revealed that **C5** and **C7** possess a *S* configuration, whereas **C6** has an *R* configuration on the stereogenic center, as depicted in Figure 1. Interestingly, complex **C7** crystallizes in the monoclinic crystal lattice in the space group *C*2 and therefore possesses symmetry operations like a two-fold rotation axis (see Figure 2).

Furthermore, all Cu^{I} complexes display a strongly distorted tetrahedral geometry around the copper center as a common feature for this class of compounds.[4,61] In the solid state structure of **C1** the two phenyl-(2-oxazoline) moieties are almost perpendicular oriented towards each other, without any perturbation in the ligand backbone. This can be visualized by the ligand plane intersection angle (lpia), which describes the angle between the two ligand planes, that are spanned through the chelating P^*N*-heteroatoms and the copper center (see Table 1).[4,61] This angle is 85.88° for complex **C1** without any substituents at the 4-position of the 2-oxazoline (Figure 3). The observed lpia is also well represented by the DFT calculations (BP86-D3(BJ)/def2-TZVP), which provide a value of 81.9° for **C1** (Table 3). For **C2**–**C7** the lpia significantly differs from the ideal 90° arrangement, for example, 71.09° (DFT, 75.4°) for **C2** or 68.01° (DFT, 68.6°) for **C6**, and is strongly influenced by the various substituents. However, a clear trend concerning the kind and size of substituents cannot be observed. Instead, the individual packing in the solid state seems to superimpose any general trend.

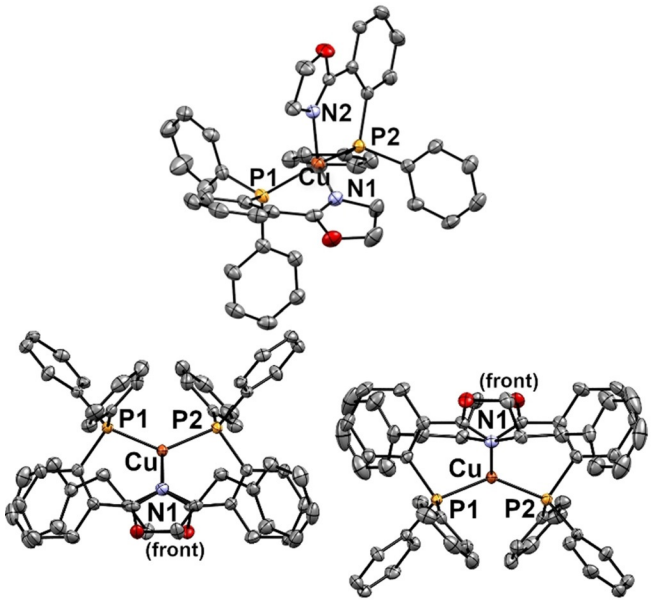

Figure 2. Solid state structures (ORTEP representation with thermal ellipsoids at a probability level of 50%) of complex **C1** with atom labeling (top) and of complex **C7** highlighting the two-fold rotation symmetry (bottom). The hydrogen atoms, counter anions and solvent molecules are omitted for clarity.

Additionally, in **C1** the copper center is asymmetrically chelated by the two **L1** ligands. One ligand is more loosely bound

Table 1. Selected crystallographic bond lengths (pm) and angles (°) of the complexes **C1**–**C7**. For atom labelling also compare with Figure 2 and the Supporting Information. The respective CCDC reference numbers are given in the supporting information. These data are provided free of charge by the Cambridge Crystallographic Data Centre.

	C1	C2	C3	C4	C5	C6	C7
space group	$P2_1/n$	$P2_1/n$	*P*4*cc*	$P2_1/n$	$P2_1$	$P2_12_12_1$	*C*2
Flack parameter	–	–	–	n.a.[a]	0.004(4)	0.012(2)	0.007(6)
Cu–P1	2.2230(8)	2.2640(8)	2.2143(10)	2.2428(4)	2.2428(4)	2.2263(8)	2.2628(15)
Cu–P2	2.1860(8)	2.2726(7)	2.2160(10)	2.2502(4)	2.2502(4)	2.2186(7)	2.2629(15)
Cu–N1	2.047(2)	2.094(2)	2.070(3)	2.0488(12)	2.0488(12)	2.071(2)	2.128(5)
Cu–N2	2.007(2)	2.070(2)	2.061(3)	2.0712(12)	2.0712(12)	2.066(2)	2.128(5)
P1-Cu-N1	91.20(8)	86.38(6)	88.39(9)	91.54(4)	91.54(4)	86.88(7)	89.24(12)
P2-Cu-N2	97.25(7)	86.98(7)	88.56(9)	87.86(4)	87.86(4)	87.81(7)	89.24(12)
plane angle[b]	85.88	71.09	73.93	77.56	78.48	68.01	88.31

[a] Not applicable, because of a centrosymmetric point group. [b] Determined ligand plane intersection angle (lpia) between the two ligand planes.

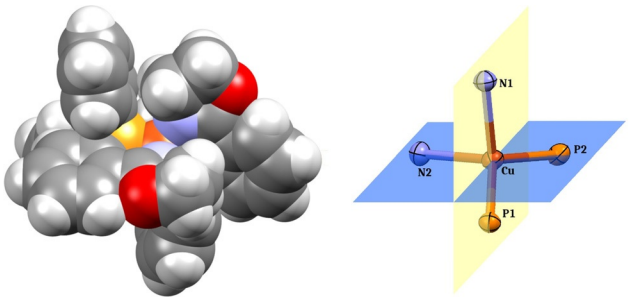

Figure 3. Space-filling representation of **C1** (left) and simplified solid state structure (right) showing only the copper center and the chelating heteroatoms (with thermal ellipsoids at a probability level of 90%). The simplified structure of **C1** displays the two ligand planes, that is, the plane through the atoms P1-Cu1-N1 (yellow) and P2-Cu1-N2 (blue).

and exhibits a bite angle of 91.20(8)°, while for the second ligand the Cu–P bond length is significantly shortened (Cu–P1: 2.2230(8) pm vs. Cu–P2: 2.1860(8) pm) and the bite angle is 97.25(7)°. A similar coordination behavior is also found for **C4** and **C5**. The detailed inspection of the extended crystal structures and crystal packing effects revealed pairwise intermolecular π-stacking interactions (Figure S4) for **C1**, **C4**, **C5** and **C7**. In **C4** and **C5**, one aryl ring of adjacent PPh_2 groups participates in a perpendicular T-shaped stacking interaction, whereas in **C1** the interaction takes place between one PPh_2 unit and the central aryl moiety in 2-position of the oxazoline. A distance of about 500 pm between the centroids of the aryl groups clearly indicates such interactions,[62–64] which are predominantly responsible for the asymmetric coordination environment. The highly symmetrical structure of **C7** also exhibits pairwise π-stacking interactions, but these are located between the substituents. Two neighboring benzyl units form an intermolecular parallel face-centered π-stacking with a centroid distance of 470 pm. Moreover, the DFT calculated ground state structures (Table 3 and Supporting Information) show a good agreement to the measured ones.

Although significantly different it is difficult to rank the substituents in terms of their steric requirements.[65] To have a more profound definition and classification of the "size of the substituent" the molecular surfaces were calculated with the GEPOL algorithm.[66] By calculating a smaller model system, that is, only considering the 4-substituted 2-oxazoline moiety (Figure S5, Table S4), the surface size follows the order **L1** < **L2** < **L3** and **L4** < **L5** < **L6** < **L7**, whereby the surface size is enlarged according to the size of the respective substituent. The same trend is observed for the case that R_1 and R_2 are similar. The surface size for **C1** < **C2** < **C3** increases with more steric demanding substituents, that is, H < Me < Ph. Interestingly, the calculated surface values, and thus, the expansion of the molecular volumes of **C4** (R_2 = *i*Pr) and **C6** (R_2 = Ph) are almost the same, but much smaller than those of **C5** (R_1 = *i*Bu) and **C7** (R_1 = Bn). This observation can be explained by the different configuration of the ligands, because in **C4** and **C6** (*S* configured) the substituents points towards each other, whereas in **C5** and **C7** (*R* configured) the substituent R_2 points to the outside of the complex (Figure 4). Hence, the steric demand of the substituents is not the crucial factor for the molecular surface. Instead the differences in chirality and the spatial arrangement are most important.

To verify these findings, an analysis of the buried volume (%V_{bur}) using the SambVca 2.0 online software[67] was carried out. This method developed by Cavallo et al. describes the space filling of the first coordination sphere in transition metal complexes.[68–70] The results (Table S5) are in line with the surface sizes obtained by the GEPOL algorithm. This means, that the complexes **C4** and **C6** employing *R* configured ligands are much more densely packed around the copper center than the complexes **C5** and **C7** with *S* configured ligands.

Electrochemical Properties

Cyclic voltammograms (CVs) of the complexes **C1**–**C7** were recorded in acetonitrile solution. Apart from **C3** all compounds display a fully reversible reduction and oxidation event each (Figure 4, Table 3). It needs to be mentioned, that the reduction in **C3** is only reversible at scan rates above 500 $mV\,s^{-1}$, whereas the oxidation stays irreversible (Figure S6). The reduc-

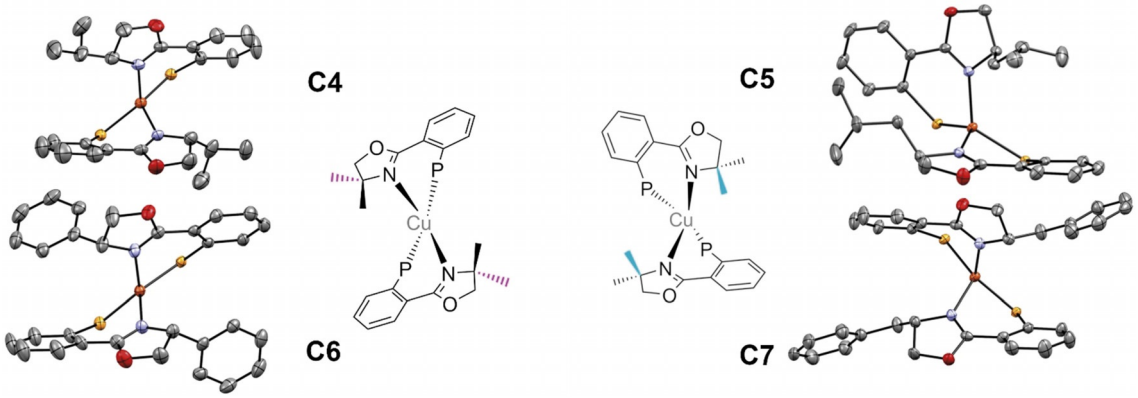

Figure 4. Simplified solid-state structures (ORTEP representation) of **C4**–**C7** highlighting the ligand orientation in the respective Cu^{I} complexes. The substituents in **C4** and **C6** point away from each other, whereas in **C5** and **C7** they point towards each other. Thermal ellipsoids are at a probability level of 50%. The hydrogen atoms, the phenyl groups of the PPh_2 moiety, counter anions and solvent molecules are omitted for clarity.

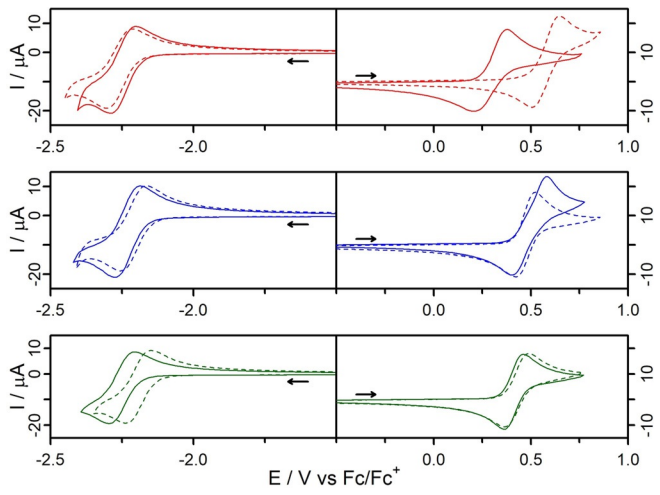

Figure 5. Cyclic voltammograms of **C1**–**C7** in acetonitrile solution referenced vs. the ferrocene/ferricenium (Fc/Fc^+) couple. Left: reductive scans. Right: oxidative scans. **C1**/**C2** (red, solid/dashed), **C4**/**C6** (blue, solid/dashed), **C5**/**C7** (green, solid/dashed), Conditions: scan rate of 100 mVs^{-1}, with 0.1 M nBu_4NPF_6 as supporting electrolyte.

tion of **C1**–**C6** occurs at potentials between −2.25 to −2.21 V and corresponds to a one-electron reduction of the P^*N*-ligand (Figure 5).[41,44,71] DFT calculations confirmed this assignment and revealed that the spin density of the reduced complex is only located at the coordinating atoms and the central aryl unit (Figure S8). Therefore, this process is largely invariant from the different substituents at the 2-oxazoline moiety, because they are not part of the conjugated system of the phox ligand. Solely in complex **C7** the reduction is slightly shifted by about 50 mV to more positive potentials.

In contrast, the reversible oxidation potentials, which formally can be assigned to a metal-centered Cu^+/Cu^{2+} oxidation process, are influenced by the substituents. The oxidation potential of **C2** (0.58 V) is shifted by 300 mV more anodic compared to that of **C1** (0.29 V). Apparently, the Cu^{II} center ([Ar] $3d^9$) in the oxidized species favors a square planar coordination environment. This flattening seems to be hampered in **C2** through the steric impact of the two methyl groups at the oxazoline moiety. This is in line with findings on Cu^I complexes with 2,9-substituted phenanthroline ligands, for example, in $[Cu(N^N)(POP)]^+$ (POP = bis[2-(diphenylphosphino)-phenyl]ether), where the complex with N^N = 2,9-dimethyl-phenanthroline shows a shift of 150 mV towards more positive potentials compared to the complex without substituents at the diimine ligand.[72] Moreover, there is a direct correlation between the oxidation potentials and the different orientations of the substituents in the chiral ligands. The complexes with a larger expansion of the molecular volumes **C4** and **C6** (0.49 V and 0.47 V) are oxidized at higher potentials compared to **C5** and **C7** (0.41 V and 0.42 V). All in all, these observations seem to be in relation to the entatic state principle,[73] which describes a pre-organization of the ligand sphere in order to stabilize a certain coordination mode. This structural pre-distortion is known for Cu^I complexes in a protein matrix,[74–76] as well as for other synthetically Cu^I complexes,[77–81] for example, Cu^I complexes with guanidine ligands[80,81] or heteroleptic Cu^I complexes with sterically demanding phenanthroline ligands.[78]

The diffusion coefficients (***D***, Table 2) were obtained from the scan rate-dependent CVs and the baseline corrected forward-scan peak potentials ($i_{p,f}$) by using the Randles-Sevcik equation (Figure S7). As a result, there seems no direct correlation between the diffusion constants and the chirality or the steric demand, because ***D*** is always about 1.13×10^{-5} cm^2s^{-1}. This is most likely due to a similar globular shape in solution for **C1**–**C7**.

Table 2. Summary of the electrochemical properties of the complexes **C1**–**C7** in acetonitrile solution at room temperature. Potentials are referenced to the ferrocene/ferricenium (Fc/Fc^+) redox couple. Diffusion coefficients *D* are determined using the Randles–Sevcik equation (see Supporting Information).

	$E^{1/2}_{red}$	$E^{1/2}_{ox}$	D [$cm^2s^{<M-1}$]
C1	−2.25	0.29	1.15×10^{-15}
C2	−2.25	0.58	1.14×10^{-5}
C3	−2.14[a,b]	0.76 [a,c]	n.d.[d]
C4	−2.23	0.49	1.13×10^{-5}
C5	−2.25	0.41	1.06×10^{-5}
C6	−2.21	0.47	1.15×10^{-5}
C7	−2.19	0.42	1.14×10^{-5}

[a] Irreversible. [b] Anodic peak. [c] Cathodic peak. [d] Not determined.

Absorption and Emission Properties

The absorption spectra of **C1**–**C7** in dichloromethane (Figure 6) are dominated by strong ligand centered (LC) transitions (π-π^* and n-π^*) in the wavelength range below 300 nm.[41] Notably, the different substituents and substitution pattern have only a marginal influence on the band shape and energy. Solely in **C6** and **C7** additional LC transitions below 270 nm, caused by the aromatic substituents, increase the extinction coefficient to some extend ($\varepsilon_{250\,nm} = 30\,000\,M^{-1}cm^{-1}$). In comparison, the complexes **C4** and **C5** with aliphatic chains in 4-position at the 2-oxazoline possess an extinction coefficient of $\varepsilon_{250\,nm} = 25\,000\,M^{-1}cm^{-1}$. The comparably weak ($\varepsilon_{400\,nm} = 1500$–$2300\,M^{-1}cm^{-1}$) and broad tails for **C1**–**C5** and **C7** in the range

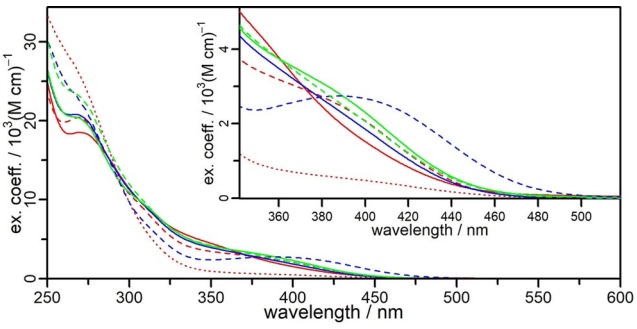

Figure 6. UV/vis absorption spectra of **C1**/**C2**/**C3** (red, solid/dashed/dotted), **C4**/**C6** (blue, solid/dashed) and **C5**/**C7** (green, solid/dashed) in dichloromethane under inert conditions. The inset is an enlargement of the MLCT region.

between 350 and 450 nm can be attributed to metal-to-ligand charge transfer (MLCT) processes.[41] The respective TD-DFT calculations of **C1** also suggest that the lowest-lying excitations are mainly involving the frontier orbitals HOMO-*n* ($n=0$, 1, 2) and LUMO$+m$ ($m=0$, 1, 2). The HOMO (as well as the HOMO-1 and HOMO-2) of both complexes corresponds to a Cu^{I} d orbital. The LUMO and LUMO$+1$ are ligand-centered orbitals, where the electron density is distributed over the coordinating nitrogen atoms and the joint of the 2-oxazoline and the central aryl ring itself. The LUMO$+2$ is mostly localized on one of the aryl substituents of the PPh_2 moiety (Figure S11b, Table S6). Consequently, the most dominant electronic transition (HOMO$\rightarrow$LUMO) can be assigned to a charge-separation from the copper center to the π^*-orbitals of the ligand sphere.[41] This is also the case for **C6**, resulting in a far more pronounced and clearly separated MLCT band from the other optical transitions (Figure S11a, Tables S6 and S7). Compared to the unsubstituted parent complex **C1**, the low-energy transitions are bathochromically shifted with a simultaneous increase in extinction coefficients (Figure 6). This observation is also reflected in the TD-DFT calculations, where the $S_0\rightarrow S_1$ and $S_0\rightarrow S_2$ transitions are shifted to lower energy compared to **C1**.

In comparison to structurally related mono- and multinuclear Cu^{I} complexes bearing P^N, P^N^P, P^N^N^P or N^P^N ligands, the low-energy bands of **C1**–**C7** are generally bathochromically shifted, for example, $[(POP)Cu(P\text{^}N)]^{+}$, where P^N = 8-diphenyl-phosphanylquinoline only exhibits an absorption maxima (shoulder) at 360 nm,[44] and $[Cu_2(PNNP)Br_2]$, with PNNP = 1,3-bis(1-(2-(diphenylphospanyl)phenyl)-1*H*-pyrazol-3-yl)benzene has also only weak absorption bands in the 325–375 nm region.[82] This renders the present Cu^{I} phosphinooxazoline complexes more attractive for light-harvesting applications. Nevertheless, the ability to harvest visible (sun)light is still inferior compared to benchmark photosensitizers like $[Ru(bpy)_3]^{2+}$ ($\lambda_{max,MLCT}=452$ nm, $\varepsilon=13.000\ M^{-1}cm^{-1}$) or [*fac*-Ir(ppy)$_3$] ($\lambda_{max}=375$ nm, $\varepsilon=7.200\ M^{-1}cm^{-1}$).[83,84] The light absorption of $[Cu(P\text{^}N)_2]^{+}$ complexes could possibly further improved by the use of larger, stiffer and sterically more demanding hetero-bidentate P^N ligands.

Only complexes **C2** and **C4–C7** show emission (Figure S9, Table 4) in deaerated dichloromethane solution at room temperature (293 K), but of very low intensity so that reliable values for the quantum yields could not be obtained. The spectra are broad and structureless with a maximum at about 600 nm, which is indicative for ^{3}MLCT states.

Excited State Structure

After excitation with light that corresponds to the wavelength of the MLCT region Cu^{I} is formally oxidized to Cu^{II} and the electron configuration changes from d^{10} to d^9. In solution, this charge transfer induces a structural reorganization from a tetrahedral geometry in the ground state (S_0) to a distorted square-planar ligand field in the singlet excited state (S_1). The related triplet excited state (T_1) exhibits a similar geometry.[41,85] To get a deeper insight into the influence of the different substituents on this flattening process, the geometries of S_0 and S_1 of **C1**–**C7** (Figures S10) were optimized at the B3LYP- D3(BJ)//def2-SVP level of theory. As described in the discussion of the crystal structures above, in the ground state the lpia of **C1**–**C7** is correlated to the steric information of the substituents, but an impact of π-stacking effects and distortions within the ligands is also present. All in all, the difference in lpia between S_0 and S_1 geometries is directly associated with the steric encumbrance of the ligand within the complex. For **C1**, which does not contain substituents at the 2-oxazoline moiety, a difference in lpia (Δlpia) between the S_0 (83.50°) and the S_1 state (45.72°) of 37.78° is the highest one of all complexes (Table 3).

Table 3. Compilation of the ligand plane intersection angle (lpia, °), reorganization energies $\Delta E_{S_1-S_0}$ and energy differences between the S_1 and T_1 state of the complexes **C1–C7** assessed from their calculated structures.

	C1	C2	C3	C4	C5	C6	C7
crystal	85.88	71.09	73.93	77.56	78.48	68.01	88.31
S_0[a]	81.88	75.35	76.03	71.89	79.91	68.59	84.10
S_0[b]	83.50	73.13	75.86	72.24	82.82	69.12	83.22
S_1[b]	45.72	56.98	59.41	41.03	66.09	38.53	68.24
$\Delta lpia^{[b]}_{S_1-S_0}$	37.78	16.15	16.45	31.21	16.73	30.59	15.00
$\Delta E^{[b]}_{S_1-S_0}$	84.45	68.85	58.85	93.94	64.84	95.95	58.41
$\Delta E^{[b]}_{T_1-S_1}$	0.15	0.17	0.13	0.17	0.16	0.17	0.15

[a] BP86-D3(BJ)//def2-TZVP. [b] B3LYP-D3(BJ)//def2-SVP.

Instead, the Δlpias are significantly lower for **C2** (4,4′-dimethyl, 16.15°) and **C3** (4,4′-diphenyl, 16.45°), but practically unaltered in these two complexes containing two substituents each. However, the energy difference between the ground and the excited state is higher in the case of **C3**. This is due to an increased steric repulsion, which limits the structural changes in the ligand sphere.

Interestingly, for the unsymmetrically and singly substituted complexes **C4**–**C7** the estimated reorganization energy is almost independent of the mass or size of the substituents, but strongly depends on the *R* and *S* configuration. TD-DFT calculations of the complexes with *R* configured ligands (i.e., **C4** and **C6**) exhibit a Δlpia of approx. 31° (Table 3). This is much larger compared to the *S* configured complexes **C5** and **C7** with a Δlpia of approx. 16°. Hence, only in **C5** and **C7**, where the substituents at adjacent ligands are pointing towards each other, the flattening distortion is hampered (for S_0 and S_1 structures see Figure S10). Another promising alternative to prevent unwanted flattening upon photoexcitation is the design of linear Cu^{I} complexes based on for example, cyclic alkyl(amino)-carbenes, *N*-heterocyclic carbenes and different pyridine or amide ligands.[86,87,88,89] The coplanar arrangement of the ligands can suppress non-radiative decay and reduce structural reorganization resulting in highly efficient Cu^{I} emitters.

Solid-State Emission and Lifetime

Unlike their behavior in solution the complexes **C2** and **C4**–**C7** are clearly luminescent in the solid state (Figure S12b) with luminescence quantum yields Φ between 0.3 to 8.5% (Table 4).

Table 4. Photophysical data of **C1–C7** in dichloromethane solution and in the solid state at room temperature under argon. Relative photoluminescence quantum yields in solution ($\phi_{PLQY,l}$) were determined using $[Ru(bpy)_3]PF_6$ as standard ($\phi_R = 0.095$ in MeCN[95,96]). Absolute photoluminescence quantum yields in the solid ($\phi_{PLQY,s}$) were determined using an integrating sphere with an experimental error of 5% of the obtained values. The excitation wavelength in all experiments was $\lambda = 355$ nm.

	λ_{em}^{DCM}	FWHM[d]	$\Phi_{PLQY,l}$	λ_{em}^{solid}	FWHM[d]	$\Phi_{PLQY,s}$	τ_{em}^{solid}
	[nm]	[nm]	[%]	[nm]	[nm]	[%]	[ns]
C1	–[a]	–[c]	–[c]	–[a]	–[c]	0.3	–[c]
C2	603	122	1.4	549	99	8.5	1329 ± 5
C3	507, 590[b]	–[c]	–[c]	585	110	0.6	666 ± 207
C4	592	146	0.18	550	95	3.6	1457 ± 12
C5	592	130	0.59	557	102	3.4	819 ± 3
C6	609	136	0.34	574	99	2.4	488 ± 6
C7	591	137	0.26	519	104	3.8	2781 ± 7

[a] The emission intensity was below the detection limit. [b] Shoulder. [c] Not determined. [d] Full width at half maximum of the emission. [e] The long-lived major lifetime component is given. For further details, see Supporting Information and ref. [97].

Upon excitation in the MLCT regime the crystalline solids of **C2** and **C4–C7** exhibit structureless emission bands with a full width at half maximum (FWHM) of about 100 nm (Table 4). Interestingly, the emission maxima are significantly hypsochromically shifted of up to 72 nm for **C7** compared to the maxima in solution. This shift can be explained by the luminescence rigodochromic effect[90] as well as by the smaller changes of the molecular geometry in the solid state upon excitation.[91] Linfoot et al. showed, that even in the solid state it is highly important to maximize the steric repulsion between the ligands and the metal center in order to increase the photoluminescence quantum yield of Cu^I complexes.[92] They studied the solid state emission of $[(POP)Cu(N\wedge N)]^+$ complexes (with POP = bis[2-(diphenyl-phosphino)-phenyl ether) and N^N = 4,4′-dimethyl- or 4,4′,6,6′-tetramethyl-2,2′-bipyridine) and found that already a methyl group largely hinders the flattening in the solid state and therefore increases the emission.[86] The same behavior is observed in our case, when changing from **C1** (no substituents) to **C2** (two methyl groups). Furthermore, the complexes **C1–C7** display an unexpected strong dependence of the solid-state emission color from the different substituents (Figure S12a). The emission covers a spectral region ranging from 519 nm in **C7** up to 585 nm for **C3**. However, there seems no clear correlation between the size or kind of the substituents and the emission maxima. In addition, emission lifetime measurements of crystalline samples of the complexes **C1–C7** were performed at room temperature. After excitation at 355 nm, **C2–C7** possess luminescence lifetimes in the sub-microsecond timescale (Table 4). **C7** exhibits the longest emission lifetime, with a long-lived component of about 2.8 μs (Table 4). The energy separation between the S_1 and T_1 state in **C1–C7** is estimated to be around 130–170 meV (Table S8). Thermally activated delayed fluorescence (TADF), however, is therefore expected to be less dominant and the emission lifetime is most likely only associated with the decay of a ^{3}MLCT state.[93,94]

Photostability and Photoreactivity

With respect to possible applications in solar energy conversion schemes a high photostability in solution is essential. Unfortunately, heteroleptic diimine-diphosphine Cu^I complexes frequently suffer from a limited stability in solution under irradiation or catalytic conditions.[31–34,98] Irradiation of the prototype photosensitizer $[(P\wedge P)Cu(N\wedge N)]PF_6$ (P^P = xantphos and N^N = bathocuproine) in acetonitrile with a solar light source (i.e., a 150 W Xe arc lamp) leads to ligand dissociation and the formation of the respective homoleptic complexes (Figure S14). In contrast, a ligand exchange reaction in the related heteroleptic complex [(**L2**)Cu(bathocuproine)]PF_6 does not occur (Figure S14). Furthermore, the homoleptic complexes **C1–C7** are not prone to changes in their molecular composition, which results in more photostable (Figure S15) complexes compared to heteroleptic Cu^I complexes bearing a P^P ligand. The photostability measurements in acetonitrile solution have also shown, that the *S* configured complexes display a slightly higher stability than the *R* configured, which can be explained by the reduced steric constraints.

In a next step, the electron transfer properties of these novel photosensitizers upon light irradiation were tested by the interaction with commonly used sacrificial reductants as well as with a water reduction catalyst.[99] For this purpose, an acetonitrile solution containing **C2** (0.1 mM) and either dimethylphenylbenzimidazoline (BIH, 0.5 mM) or triethylamine (TEA, 100 mM) was irradiated. Simultaneous UV/vis measurements revealed the constant build-up of a new band at 570 nm (Figure S16). The speed and magnitude of interaction using TEA, however, is substantially slower than with BIH, which is in accordance with the lower oxidation potential of BIH.[99] The interplay of **C2** with a water reduction catalyst was probed with the commonly used iron carbonyl complex $[Fe_3(CO)_{12}]$[6,7,35,41] (Figure S17). From the Stern–Volmer experiment, an apparent emission quenching can be seen ($K_{SV} = 1.99 \times 10^3\ M^{-1}$). These spectroscopic observations are in line with our previous results, where complex **C2** was used for the light-driven reduction of protons to hydrogen within a fully noble-metal-free system composed of $[Fe_3(CO)_{12}]$ as water reduction catalyst and triethylamine as sacrificial reductant.[41] There, **C2** showed a low, but fairly constant production of H_2 with a turnover number of 53 within 24 h.[41]

Conclusions

Based on the phosphinooxazoline ligand a systematic series of sterically modified P^N ligands **L1–L7**, without any substituents (**L1**), with only one substituent (**L4–L7**) and two substituents (**L2–L3**) at the 2-oxazoline moiety, were prepared. These heterobidentate P^N ligands were then used to design a new class of homoleptic Cu^I photosensitizers **C1–C7** and to study their impact on the photophysical and electrochemical properties. The different ligands are either available by a two-step procedure starting from the commercially available amino alcohols or via a three-step synthesis using natural amino acids. The complexes **C1–C7** (yellow to orange solids) were mostly

obtained in good yields with a remarkably photostability in solution. A comprehensive X-ray analysis revealed a uniform coordination behavior around the copper center and exposed major differences of the ligand arrangement in *S* and *R* substituted complexes.

The redox processes of all complexes (except **C3**) are fully reversible, which is in strong contrast to most of the conventional heteroleptic diamine-diphosphine Cu^{I} photosensitizers. While the reduction potentials are not affected by the different substituents or substitution pattern, the oxidation of **C2**–**C7** occurs at higher potentials compared to **C1**, which does not bear any substituents. The absorption spectra are largely unaffected by the different substituents, with only complex **C6** having a phenyl substituent exhibiting a pronounced bathochromic shift of the MLCT band. (TD-)DFT calculations corroborate the findings and were used to determine the excited state structures. The respective MLCT state undergoes a strong flattening distortion, which is independent of the specific kind, size or number of substituents. Instead, the specific properties are dictated by the chirality of the ligands. Furthermore, the flattening distortion is the main reason for the weak emission in solution. In contrast, all complexes show a clear emission in the solid state with a dependence of the emission color on the steric information. Additionally, the successful interaction of **C2** with sacrificial reductants as well as with an iron carbonyl water reduction catalyst was demonstrated. As another key advantage compared to heteroleptic diimine-diphosphine Cu^{I} photosensitizers these novel $[Cu(N\text{^}P)_2]^{+}$ complexes were found to be quite photorobust and do not suffer from photoinduced ligand exchange reactions in solution.

All in all, this renders these class of compounds as suitable for various applications within solar energy conversion schemes. At the same time, this study highlights the importance of having control over chirality and steric information in Cu^{I} complexes. In the future, multidentate N^N^P or P^N^N^P ligands[100] as well as macrocyclic phenanthroline ligands[36] might be used as suitable alternatives to P^N ligands to further improve Cu^{I} based photosensitizers.

Experimental Section

CCDC CCDC 1934742 (**C1**), 11561237 (**C2**), 1934740 (**C3**), 1934739 (**C4**), 1947485 (**C5**), 1947486 (**C6**), and 1934741 (**C7**) contain the supplementary crystallographic data for this paper. These data are provided free of charge by The Cambridge Crystallographic Data Centre.

Acknowledgements

This work was supported by the Deutsche Forschungsgemeinschaft (DFG, Priority Program SPP 2102 "Light-controlled reactivity of metal complexes" (TS 330/4-1, STE 1834/7-1 and KA 4671/2-1)) and the DFG project TS 330/3-1. M.K. and S.T. are grateful to the Fonds der Chemischen Industrie (FCI) for funding. The authors also acknowledge support by the state of Baden-Württemberg through bwHPC and by the DFG (INST 40/467-1 FUGG). We thank Benedikt Bagemihl for assistance in the lab.

Conflict of interest

The authors declare no conflict of interest.

Keywords: copper complexes · photophysics · P^N ligands · structure–property relations · X-ray structures

[1] Y.-J. Yuan, Z.-T. Yu, D.-Q. Chen, Z.-G. Zou, *Chem. Soc. Rev.* **2017**, *46*, 603 – 631.
[2] Y. Liu, S.-C. Yiu, C.-L. Ho, W.-Y. Wong, *Coord. Chem. Rev.* **2018**, *375*, 514 – 557.
[3] M. S. Lazorski, F. N. Castellano, *Polyhedron* **2014**, *82*, 57 – 70.
[4] Y. Zhang, M. Schulz, M. Wächtler, M. Karnahl, B. Dietzek, *Coord. Chem. Rev.* **2018**, *356*, 127 – 146.
[5] M. Sandroni, Y. Pellegrin, F. Odobel, *C. R. Chim.* **2016**, *19*, 79 – 93.
[6] S.-P. Luo, E. Mejía, A. Friedrich, A. Pazidis, H. Junge, A.-E. Surkus, R. Jackstell, S. Denurra, S. Gladiali, S. Lochbrunner, M. Beller, *Angew. Chem. Int. Ed.* **2013**, *52*, 419 – 423; *Angew. Chem.* **2013**, *125*, 437 – 441.
[7] E. Mejía, S.-P. Luo, M. Karnahl, A. Friedrich, S. Tschierlei, A.-E. Surkus, H. Junge, S. Gladiali, S. Lochbrunner, M. Beller, *Chem. Eur. J.* **2013**, *19*, 15972 – 15978.
[8] J. Kim, D. R. Whang, S. Y. Park, *ChemSusChem* **2017**, *10*, 1883 – 1886.
[9] S. Saeedi, C. Xue, B. J. McCullough, S. E. Roe, B. J. Neyhouse, T. A. White, *ACS Appl. Energy Mater.* **2019**, *2*, 131 – 143.
[10] J. Windisch, M. Orazietti, P. Hamm, R. Alberto, B. Probst, *ChemSusChem* **2016**, *9*, 1719 – 1726.
[11] R. S. Khnayzer, C. E. McCusker, B. S. Olaiya, F. N. Castellano, *J. Am. Chem. Soc.* **2013**, *135*, 14068 – 14070.
[12] K. Matsuo, E. Yamaguchi, A. Itoh, *Asian J. Org. Chem.* **2018**, *7*, 2435 – 2438.
[13] O. Reiser, *Acc. Chem. Res.* **2016**, *49*, 1990 – 1996.
[14] S. Paria, O. Reiser, *ChemCatChem* **2014**, *6*, 2477 – 2483.
[15] B. M. Hockin, C. Li, N. Robertson, E. Zysman-Colman, *Catal. Sci. Technol.* **2019**, *9*, 889 – 915.
[16] B. Wang, D. P. Shelar, X.-Z. Han, T.-T. Li, X. Guan, W. Lu, K. Liu, Y. Chen, W.-F. Fu, C.-M. Che, *Chem. Eur. J.* **2015**, *21*, 1184 – 1190.
[17] M. Wallesch, D. Volz, D. M. Zink, U. Schepers, M. Nieger, T. Baumann, S. Bräse, *Chem. Eur. J.* **2014**, *20*, 6578 – 6590.
[18] B. Jiao, J. Wang, J. Huang, M. Cao, C. Liu, G. Yin, Y. Zhu, B. Zhang, C. Du, *Org. Electron.* **2019**, *64*, 158 – 165.
[19] E. Cariati, E. Lucenti, C. Botta, U. Giovanella, D. Marinotto, S. Righetto, *Coord. Chem. Rev.* **2016**, *306*, 566 – 614.
[20] M. Wallesch, A. Verma, C. Fléchon, H. Flügge, D. M. Zink, S. M. Seifermann, J. M. Navarro, T. Vitova, J. Göttlicher, R. Steininger, L. Weinhardt, M. Zimmer, M. Gerhards, C. Heske, S. Bräse, T. Baumann, D. Volz, *Chem. Eur. J.* **2016**, *22*, 16400 – 16405.
[21] F. Dumur, *Org. Electron.* **2015**, *21*, 27 – 39.
[22] C. Bizzarri, E. Spuling, D. M. Knoll, D. Volz, S. Bräse, *Coord. Chem. Rev.* **2018**, *373*, 49 – 82.
[23] S. Y. Brauchli, E. C. Constable, C. E. Housecroft, *Dyes Pigm.* **2015**, *113*, 447 – 450.
[24] E. Schönhofer, B. Bozic-Weber, C. J. Martin, E. C. Constable, C. E. Housecroft, J. A. Zampese, *Dyes Pigm.* **2015**, *115*, 154 – 165.
[25] C. E. Housecroft, E. C. Constable, *Chem. Soc. Rev.* **2015**, *44*, 8386 – 8398.
[26] B. Bozic-Weber, E. C. Constable, C. E. Housecroft, *Coord. Chem. Rev.* **2013**, *257*, 3089 – 3106.
[27] R. D. Costa, D. Tordera, E. Ortí, H. J. Bolink, J. Schönle, S. Graber, C. E. Housecroft, E. C. Constable, J. A. Zampese, *J. Mater. Chem.* **2011**, *21*, 16108 – 16118.
[28] E. Fresta, R. D. Costa, *J. Mater. Chem. C* **2017**, *5*, 5643 – 5675.
[29] A. J. J. Lennox, S. Fischer, M. Jurrat, S.-P. Luo, N. Rockstroh, H. Junge, R. Ludwig, M. Beller, *Chem. Eur. J.* **2016**, *22*, 1233 – 1238.
[30] A. Barbieri, G. Accorsi, N. Armaroli, *Chem. Commun.* **2008**, 2185 – 2193.

[31] M. Nishikawa, D. Kakizoe, Y. Saito, T. Ohishi, T. Tsubomura, *Bull. Chem. Soc. Jpn.* **2017**, *90*, 286 – 288.
[32] Y. Zhang, M. Heberle, M. Wächtler, M. Karnahl, B. Dietzek, *RSC Adv.* **2016**, *6*, 105801 – 105805.
[33] S. Fischer, D. Hollmann, S. Tschierlei, M. Karnahl, N. Rockstroh, E. Barsch, P. Schwarzbach, S.-P. Luo, H. Junge, M. Beller, S. Lochbrunner, R. Ludwig, A. Brückner, *ACS Catal.* **2014**, *4*, 1845 – 1849.
[34] A. Kaeser, M. Mohankumar, J. Mohanraj, F. Monti, M. Holler, J.-J. Cid, O. Moudam, I. Nierengarten, L. Karmazin-Brelot, C. Duhayon, B. Delavaux-Nicot, N. Armaroli, J.-F. Nierengarten, *Inorg. Chem.* **2013**, *52*, 12140 – 12151.
[35] M. Heberle, S. Tschierlei, N. Rockstroh, M. Ringenberg, W. Frey, H. Junge, M. Beller, S. Lochbrunner, M. Karnahl, *Chem. Eur. J.* **2017**, *23*, 312 – 319.
[36] M. Mohankumar, M. Holler, E. Meichsner, J. F. Nierengarten, F. Niess, J. P. Sauvage, B. Delavaux-Nicot, E. Leoni, F. Monti, J. M. Malicka, M. Cocchi, E. Bandini, N. Armaroli, *J. Am. Chem. Soc.* **2018**, *140*, 2336 – 2347.
[37] E. Leoni, J. Mohanraj, M. Holler, M. Mohankumar, I. Nierengarten, F. Monti, A. Sournia-Saquet, B. Delavaux-Nicot, J.-F. Nierengarten, N. Armaroli, *Inorg. Chem.* **2018**, *57*, 15537 – 15549.
[38] M. Alkan-Zambada, S. Keller, L. Martínez-Sarti, A. Prescimone, J. M. Junquera-Hernández, E. C. Constable, H. J. Bolink, M. Sessolo, E. Ortí, C. E. Housecroft, *J. Mater. Chem. C* **2018**, *6*, 8460 – 8471.
[39] N. S. Murray, S. Keller, E. C. Constable, C. E. Housecroft, M. Neuburger, A. Prescimone, *Dalton Trans.* **2015**, *44*, 7626 – 7633.
[40] R. Molteni, K. Edkins, M. Haehnel, A. Steffen, *Organometallics* **2016**, *35*, 629 – 640.
[41] R. Giereth, W. Frey, H. Junge, S. Tschierlei, M. Karnahl, *Chem. Eur. J.* **2017**, *23*, 17432 – 17437.
[42] M. K. Rong, F. Holtrop, J. C. Slootweg, K. Lammertsma, *Coord. Chem. Rev.* **2019**, *382*, 57 – 68.
[43] E. I. Musina, A. V. Shamsieva, I. D. Strelnik, T. P. Gerasimova, D. B. Krivolapov, I. E. Kolesnikov, E. V. Grachova, S. P. Tunik, C. Bannwarth, S. Grimme, S. A. Katsyuba, A. A. Karasik, O. G. Sinyashin, *Dalton Trans.* **2016**, *45*, 2250 – 2260.
[44] L. Qin, Q. Zhang, W. Sun, J. Wang, C. Lu, Y. Cheng, L. Wang, *Dalton Trans.* **2009**, 9388 – 9391.
[45] T. Suzuki, H. Yamaguchi, A. Hashimoto, K. Nozaki, M. Doi, N. Inazumi, N. Ikeda, S. Kawata, M. Kojima, H. D. Takagi, *Inorg. Chem.* **2011**, *50*, 3981 – 3987.
[46] D. M. Zink, M. Bächle, T. Baumann, M. Nieger, M. Kühn, C. Wang, W. Klopper, U. Monkowius, T. Hofbeck, H. Yersin, S. Bräse, *Inorg. Chem.* **2013**, *52*, 2292 – 2305.
[47] D. M. Zink, T. Baumann, J. Friedrichs, M. Nieger, S. Bräse, *Inorg. Chem.* **2013**, *52*, 13509 – 13520.
[48] A. J. M. Miller, J. L. Dempsey, J. C. Peters, *Inorg. Chem.* **2007**, *46*, 7244 – 7246.
[49] A. Neshat, R. B. Aghakhanpour, P. Mastrorilli, S. Todisco, F. Molani, A. Wojtczak, *Polyhedron* **2018**, *154*, 217 – 228.
[50] R. Mondal, I. B. Lozada, R. L. Davis, J. A. G. Williams, D. E. Herbert, *J. Mater. Chem. C* **2019**, *7*, 3772 – 3778.
[51] F. Wei, X. Liu, Z. Liu, Z. Bian, Y. Zhao, C. Huang, *CrystEngComm* **2014**, *16*, 5338 – 5344.
[52] D. M. Zink, D. Volz, T. Baumann, M. Mydlak, H. Flügge, J. Friedrichs, M. Nieger, S. Bräse, *Chem. Mater.* **2013**, *25*, 4471 – 4486.
[53] Z. Liu, P. I. Djurovich, M. T. Whited, M. E. Thompson, *Inorg. Chem.* **2012**, *51*, 230 – 236.
[54] S. Maggini, *Coord. Chem. Rev.* **2009**, *253*, 1793 – 1832.
[55] D. Volz, M. Nieger, J. Friedrichs, T. Baumann, S. Bräse, *Inorg. Chem. Commun.* **2013**, *37*, 106 – 109.
[56] M. Wallesch, M. Nieger, D. Volz, S. Bräse, *Inorg. Chem. Commun.* **2017**, *86*, 232 – 240.
[57] C. Zeng, N. Wang, T. Peng, S. Wang, *Inorg. Chem.* **2017**, *56*, 1616 – 1625.
[58] J. Sedelmeier, T. Hammerer, C. Bolm, *Org. Lett.* **2008**, *10*, 917 – 920.
[59] K. Tani, D. C. Behenna, R. M. McFadden, B. M. Stoltz, *Org. Lett.* **2007**, *9*, 2529 – 2531.
[60] D. A. Dickman, A. I. Meyers, G. A. Smith, R. E. Gawley, *Org. Synth.* **1985**, *63*, 136.
[61] N. Armaroli, G. Accorsi, F. Cardinali, A. Listorti, *Top. Curr. Chem.* **2007**, *280*, 69 – 115.
[62] C. R. Martinez, B. L. Iverson, *Chem. Sci.* **2012**, *3*, 2191 – 2201.
[63] M. O. Sinnokrot, C. D. Sherrill, *J. Am. Chem. Soc.* **2004**, *126*, 7690 – 7697.
[64] S. K. Burley, G. A. Petsko, *Science* **1985**, *229*, 23 – 28.
[65] M. K. Eggleston, D. R. McMillin, K. S. Koenig, A. J. Pallenberg, *Inorg. Chem.* **1997**, *36*, 172 – 176.
[66] J. L. Pascual-ahuir, E. Silla, I. Tuñon, *J. Comput. Chem.* **1994**, *15*, 1127 – 1138.
[67] L. Falivene, R. Credendino, A. Poater, A. Petta, L. Serra, R. Oliva, V. Scarano, L. Cavallo, *Organometallics* **2016**, *35*, 2286 – 2293.
[68] A. Poater, F. Ragone, S. Giudice, C. Costabile, R. Dorta, S. P. Nolan, L. Cavallo, *Organometallics* **2008**, *27*, 2679 – 2681.
[69] A. Poater, F. Ragone, R. Mariz, R. Dorta, L. Cavallo, *Chem. Eur. J.* **2010**, *16*, 14348 – 14353.
[70] H. Clavier, S. P. Nolan, *Chem. Commun.* **2010**, *46*, 841 – 861.
[71] J.-J. Cid, J. Mohanraj, M. Mohankumar, M. Holler, F. Monti, G. Accorsi, L. Karmazin-Brelot, I. Nierengarten, J. M. Malicka, M. Cocchi, B. Delavaux-Nicot, N. Armaroli, J.-F. Nierengarten, *Polyhedron* **2014**, *82*, 158 – 172.
[72] D. G. Cuttell, S.-M. Kuang, P. E. Fanwick, D. R. McMillin, R. A. Walton, *J. Am. Chem. Soc.* **2002**, *124*, 6 – 7.
[73] P. Comba, *Coord. Chem. Rev.* **2000**, *200 – 202*, 217 – 245.
[74] R. J. P. Williams, *Inorg. Chim. Acta* **1971**, *5*, 137 – 155.
[75] R. J. P. Williams, *J. Mol. Catal.* **1985**, *30*, 1 – 26.
[76] L. B. LaCroix, S. E. Shadle, Y. Wang, B. A. Averill, B. Hedman, K. O. Hodgson, E. I. Solomon, *J. Am. Chem. Soc.* **1996**, *118*, 7755 – 7768.
[77] G. Chaka, J. L. Sonnenberg, H. B. Schlegel, M. J. Heeg, G. Jaeger, T. J. Nelson, L. A. Ochrymowycz, D. B. Rorabacher, *J. Am. Chem. Soc.* **2007**, *129*, 5217 – 5227.
[78] L. Kohler, R. G. Hadt, D. Hayes, L. X. Chen, K. L. Mulfort, *Dalton Trans.* **2017**, *46*, 13088 – 13100.
[79] B. Dicke, A. Hoffmann, J. Stanek, M. S. Rampp, B. Grimm-Lebsanft, F. Biebl, D. Rukser, B. Maerz, D. Göries, M. Naumova, M. Biednov, G. Neuber, A. Wetzel, S. M. Hofmann, P. Roedig, A. Meents, J. Bielecki, J. Andreasson, K. R. Beyerlein, H. N. Chapman, C. Bressler, W. Zinth, M. Rübhausen, S. Herres-Pawlis, *Nat. Chem.* **2018**, *10*, 355 – 362.
[80] A. Hoffmann, S. Binder, A. Jesser, R. Haase, U. Flörke, M. Gnida, M. S. Stagni, W. Meyer-Klaucke, B. Lebsanft, L. E. Grünig, S. Schneider, M. Hashemi, A. Goos, A. Wetzel, M. Rübhausen, S. Herres-Pawlis, *Angew. Chem. Int. Ed.* **2014**, *53*, 299 – 304; *Angew. Chem.* **2014**, *126*, 305 – 310.
[81] D. F. Schrempp, S. Leingang, M. Schnurr, E. Kaifer, H. Wadepohl, H.-J. Himmel, *Chem. Eur. J.* **2017**, *23*, 13607 – 13611.
[82] J.-H. Jia, X.-L. Chen, J.-Z. Liao, D. Liang, M.-X. Yang, R. Yu, C.-Z. Lu, *Dalton Trans.* **2019**, *48*, 1418 – 1426.
[83] A. Juris, V. Balzani, F. Barigelletti, S. Campagna, P. Belser, A. Von Zelewsky, *Coord. Chem. Rev.* **1988**, *84*, 85 – 277.
[84] L. Flamigni, A. Barbieri, C. Sabatini, B. Ventura, *Top. Curr. Chem.* **2007**, *281*, 143 – 203.
[85] S. Tschierlei, M. Karnahl, N. Rockstroh, H. Junge, M. Beller, S. Lochbrunner, *ChemPhysChem* **2014**, *15*, 3709 – 3713.
[86] D. Di, A. S. Romanov, L. Yang, J. M. Richter, J. P. H. Rivett, S. Jones, T. H. Thomas, M. A. Jalebi, R. H. Friend, M. Linnolahti, M. Bochmann, D. Credgington, *Science* **2017**, *356*, 159 – 163.
[87] M. Gernert, U. Meller, M. Haehnel, J. Pflaum, A. Steffen, *Chem. Eur. J.* **2017**, *23*, 2206 – 2216.
[88] R. Hamze, J. L. Peltier, D. Sylvinson, M. Jung, J. Cardenas, R. Haiges, M. Soleilhavoup, R. Jazzar, P. I. Djurovich, G. Bertrand, M. E. Thompson, *Science* **2019**, *363*, 601 – 606.
[89] J. Föller, C. Ganter, A. Steffen, C. M. Marian, *Inorg. Chem.* **2019**, *58*, 5446 – 5456.
[90] A. J. Lees, *Comments Inorg. Chem.* **1995**, *17*, 319 – 346.
[91] A. Stoïanov, C. Gourlaouen, S. Vela, C. Daniel, *J. Phys. Chem. A* **2018**, *122*, 1413 – 1421.
[92] C. L. Linfoot, M. J. Leitl, P. Richardson, A. F. Rausch, O. Chepelin, F. J. White, H. Yersin, N. Robertson, *Inorg. Chem.* **2014**, *53*, 10854 – 10861.
[93] R. Czerwieniec, M. J. Leitl, H. H. H. Homeier, H. Yersin, *Coord. Chem. Rev.* **2016**, *325*, 2 – 28.
[94] R. Czerwieniec, H. Yersin, *Inorg. Chem.* **2015**, *54*, 4322 – 4327.
[95] H. Ishida, S. Tobita, Y. Hasegawa, R. Katoh, K. Nozaki, *Coord. Chem. Rev.* **2010**, *254*, 2449 – 2458.
[96] K. Suzuki, A. Kobayashi, S. Kaneko, K. Takehira, T. Yoshihara, H. Ishida, Y. Shiina, S. Oishi, S. Tobita, *Phys. Chem. Chem. Phys.* **2009**, *11*, 9850 – 9860.

[97] M.-A. Schmid, M. Rentschler, W. Frey, S. Tschierlei, M. Karnahl, *Inorganics* **2018**, *6*, 134.
[98] M. Holler, B. Delavaux-Nicot, J.-F. Nierengarten, *Chem. Eur. J.* **2019**, *25*, 4543 – 4550.
[99] Y. Pellegrin, F. Odobel, *C. R. Chim.* **2017**, *20*, 283 – 295.
[100] H. Chen, L.-X. Xu, L.-J. Yan, X.-F. Liu, D.-D. Xu, X.-C. Yu, J.-X. Fan, Q.-A. Wu, S.-P. Luo, *Dyes Pigm.* **2020**, *173*, 108000.

Manuscript received: September 24, 2019
Accepted manuscript online: November 20, 2019
Version of record online: February 25, 2020

